

Changes in column aerosol optical depth and ground-level particulate matter concentration over East Asia

Jihyun Nam¹ · Sang-Woo Kim¹ · Rokjin J. Park¹ · Jin-Soo Park² · Sang Seo Park¹

Received: 25 July 2017 / Accepted: 14 September 2017 / Published online: 26 September 2017
© Springer Science+Business Media B.V. 2017

Abstract Different spatio-temporal variations and trends in column aerosol optical depth (AOD) and surface particulate matter (PM₁₀; diameter < 10 μm) mass concentration were found for selected regions of East Asia. Enhanced AOD over North China and its downwind regions (Yellow Sea, Korea) occurred in June, compared with March–April over South China. Increased PM₁₀ concentration in both North and South China was observed from late fall to spring. In Northeast China, a peak in AOD appeared during March, but high PM₁₀ concentrations occurred in December–January. A significantly increasing trend in AOD was found in North and Northeast China, whereas surface PM₁₀ concentrations over most megacities in these two regions declined almost linearly. This contradictory trend between AOD and PM₁₀ concentration can be attributed to large emissions reductions in near-surface coarse particles, mainly accredited to a series of strict control measures. In other words, there has been no meaningful reduction in fine-mode particles including secondary aerosols. On the other hand, space-based CALIOP measurements revealed that approximately 60~70% (40~50%) of AOD was contributed by the aerosols present above 1 km (above 2 km) altitude. Our findings suggest that stronger emission controls for precursor gaseous emissions as

well as submicron particles are required to decrease particulate air pollution, so as to further reduce their radiative forcing.

Keywords Aerosol optical depth · Particulate matter · Trend · East Asia · MODIS

Introduction

The frequency of severe haze episodes in East Asia has increased substantially over recent decades due to increased pollutant emissions, especially under stagnant meteorological conditions favoring high secondary aerosol formation and accumulation (Cai et al. 2017; Kim et al. 2016; Lu et al. 2016; Wang and Chen 2016; Yu et al. 2011; Zhang et al. 2015). Levels of fine particulate matter during such events cause adverse human health effects, reduce visibility, and change radiation budget (Oberdörster et al. 2005; Peel et al. 2013; Zheng et al. 2015).

Ground-level particulate matter (PM) mass concentration, either PM₁₀ (diameter < 10 μm) or PM_{2.5} (diameter < 2.5 μm), is used to indicate particulate air pollution, because such particles can be inhaled by humans and cause respiratory diseases (Liu et al. 2016; Mehta et al. 2013; O'Neill et al. 2012; Yin et al. 2017). Aerosol optical depth (AOD), which is a quantitative measure of the extinction of solar radiation by the column-integrated aerosol load, is also widely used, not only to understand how the Earth's climate is radiatively forced (Kim et al. 2008; Shindell et al. 2013; Schulz et al. 2006), but also for air quality purposes, in particular with regard to regional hotspots of particulate pollution, because of its large-scale spatial measurements by satellites (Chew et al. 2016; Engel-Cox et al. 2006; Kim et al. 2007). A number of recent papers have demonstrated the strong possibility of deriving surface PM concentrations from satellite-based AOD

Electronic supplementary material The online version of this article (<https://doi.org/10.1007/s11869-017-0517-5>) contains supplementary material, which is available to authorized users.

✉ Sang-Woo Kim
sangwookim@snu.ac.kr

¹ School of Earth and Environmental Science, Seoul National University, Seoul 08826, South Korea

² National Institute of Environmental Research, Incheon 22689, South Korea

measurements to overcome the spatial limitations of ground-level PM₁₀ and PM_{2.5} concentration measurements (Lv et al. 2016; Ma et al. 2014; Seo et al. 2015; You et al. 2015; Zheng et al. 2015).

Despite the increasing trend of severe haze events and increased pollutant emissions, several studies indicated declining trends for surface PM concentrations in China and Korea over the past decades due to continued emission control efforts (Cheng et al. 2013; Qu et al. 2010; Wang et al. 2014). In contrast, satellite observations and model simulations showed an increasing trend in AOD over East Asia (Pozzer et al. 2015; Streets et al. 2009; Yu et al. 2011; Zhang and Reid 2010).

Although many studies have reported qualitative changes in PM concentration and AOD, the estimated trends depend significantly on the data period, and some discrepancies have been found for certain areas. In this study, therefore, we investigate spatial–temporal variations and trends for column aerosol AOD and surface PM₁₀ concentration during 2004–2011 for six selected regions of interest in East Asia. Descriptions for PM₁₀ and AOD data and the trend analysis method are given in the “Data and trend analysis” section. The “Results and discussion” section discusses the observed trends of PM₁₀ concentrations and AOD and their causes, with spatial and temporal variations for the six selected regions. Finally, the research findings are summarized in the “Summary and conclusion” section.

Data and trend analysis

Monthly mean AOD and Ångström exponent (ÅE) from Moderate Resolution Imaging Spectroradiometer (MODIS, collection 6) onboard Aqua were analyzed, which were derived from the most recently updated land (algorithm; dark-target and deep blue) and ocean aerosol algorithms (Levy et al. 2013; Remer et al. 2005). To further ensure the data quality, MODIS AOD were cross-checked with ground-level AOD observed at Aerosol Robotic Network (AERONET) stations in East Asia.

PM₁₀ concentrations calculated from the air pollution index (API) recorded at 27 Chinese urban stations during 2004–2011 were used in this study. Zhang et al. (2003) provide detailed descriptions for calculating PM₁₀ concentrations from APIs and their validation. It should be noted that PM₁₀ concentrations after 2012 are not used in this study, because the PM₁₀ concentration data extracted from the air quality index (AQI) were inconsistent with API. PM₁₀ concentrations at six stations in Korea and Japan during 2004–2014 were directly measured using the β -ray attenuation method, which follows the US EPA automated equivalent PM₁₀ method (EQPM-1102-150).

Trends in AOD and PM₁₀ concentration were calculated by Weatherhead’s least mean square (LMS) fit method (Eq. 1),

which has been widely used for estimating long-term trends in aerosol characteristics (Collaud Coen et al. 2013; Streets et al. 2009; Weatherhead et al. 1998).

$$Y_t = m + \rho \cdot X_t + S_t + A_t, \quad t = 1 \dots n \quad (1)$$

Here, Y_t represents monthly mean aerosol variables, t is time (months), m is a constant, ρ is the magnitude of the trend per year, and $X_t (=t/12)$ represents the linear trend function. S_t ($= \sum_{j=1}^4 [\beta_{1,j} \sin(2\pi jt/12) + \beta_{2,j} \cos(2\pi jt/12)]$) is the seasonal component, where $\beta_{1,j}$ and $\beta_{2,j}$ are seasonal variation parameters. The noise term $A_t (= \alpha \cdot A_{t-1} + \varepsilon_t)$ is modeled as autoregressive of the order of 1. Here, α is the autocorrelation coefficient of the data noise, and ε_t represents independent random variables with mean zero and common variance σ_ε^2 . The trend is statistically significant at the 5% significance level (95% confidence level) when $|\rho/\sigma_\rho|$ is > 2 (Tiao et al. 1990). Here, σ_ρ (the standard deviation of the slope) is calculated by Eq. (2):

$$\sigma_\rho \cong \frac{\sigma_\varepsilon}{(1-\alpha)} \frac{1}{n^{1.5}} = \frac{\sigma_A}{n^{1.5}} \sqrt{\frac{1+\alpha}{1-\alpha}} \quad (2)$$

σ_ε is the standard deviation of ε_t , σ_A is the standard deviation of A_t , and n is the number of years.

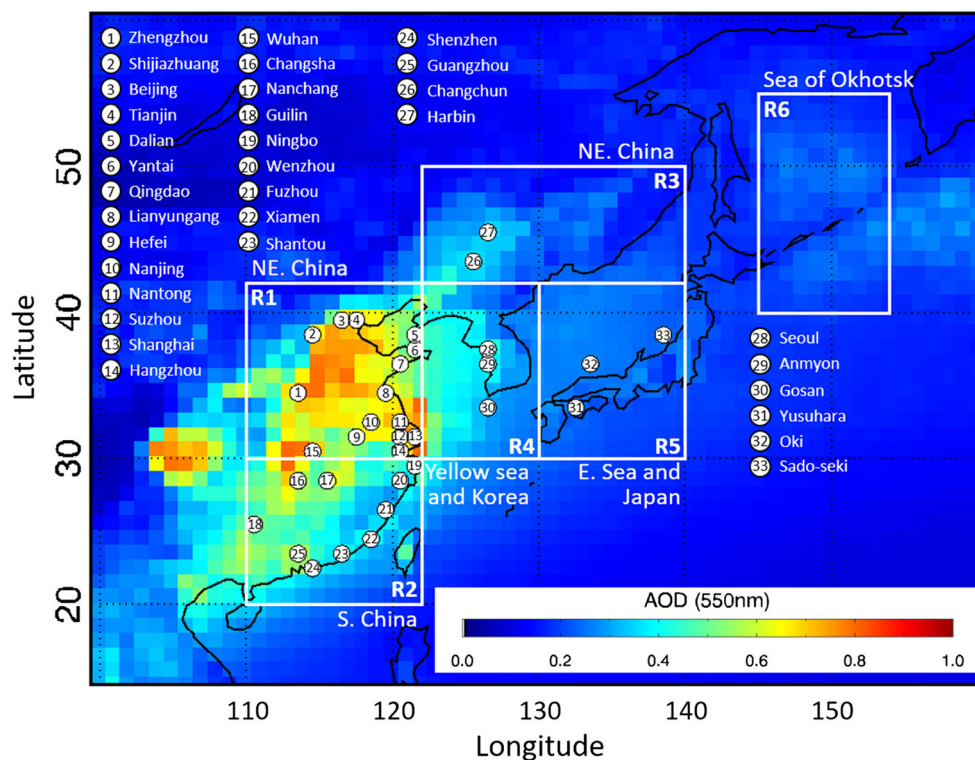
Results and discussion

Spatial and temporal variations in AOD and PM₁₀ concentration

Figure 1 shows 11-year (2004–2014) averaged MODIS AOD at 550-nm wavelength with the locations of surface PM₁₀ concentration monitoring stations. In this study, we investigate changes in columnar aerosol properties in six regions (R1, North China; R2, South China; R3, Northeast China; R4, Yellow Sea and Korea Peninsula; R5, East Sea and Japan; and R6, Sea of Okhotsk), which are chosen based on the temporal variability of aerosols related to synoptic meteorological patterns, as well as emissions (Figs. S1 and S2).

The highest annual mean AOD (0.65 ± 0.17) was observed at R1, mainly due to the heavy influence of aerosol pollutants emitted from several megacities (e.g., Beijing, Tianjin, and Hefei) and industrial complexes all year round (Chan and Yao 2008). Additionally, dust particles transported from deserts in Inland China and Mongolia contributed to elevation of AOD especially in spring (Qu et al. 2010). The annual mean AOD in R2 (0.50 ± 0.12) was lower than that observed in R1, resulting from more precipitation over R2 (Fig. S2). AOD over R3 (0.28 ± 0.13) was affected by dust particles from deserts (Nguyen et al. 2015), pollution aerosols from R1 by

Fig. 1 MODIS-derived AOD at 550-nm wavelength over East Asia averaged across 2004–2014. The boxes and circled numbers represent the six regions and ground stations, respectively



southwesterly winds (Fig. S1), and aerosols from biomass burning originating from Mongolia/Russia and R3 (Fig. 3). R4, which is adjacent to the downwind side of R1, showed an annual mean AOD of 0.41 ± 0.12 . Similar AODs were reported in R5 (0.29 ± 0.10) and R6 (0.26 ± 0.16). While column aerosol loadings in R5 are likely due to aerosols transported mainly from R1 and R4 (Kim et al. 2007), the lowest AOD featured in R6 appeared to be influenced by sea salt and biomass burning aerosols transported from R3 and from grasslands and forests in Mongolia and Russia, especially during April–July (Fig. 3).

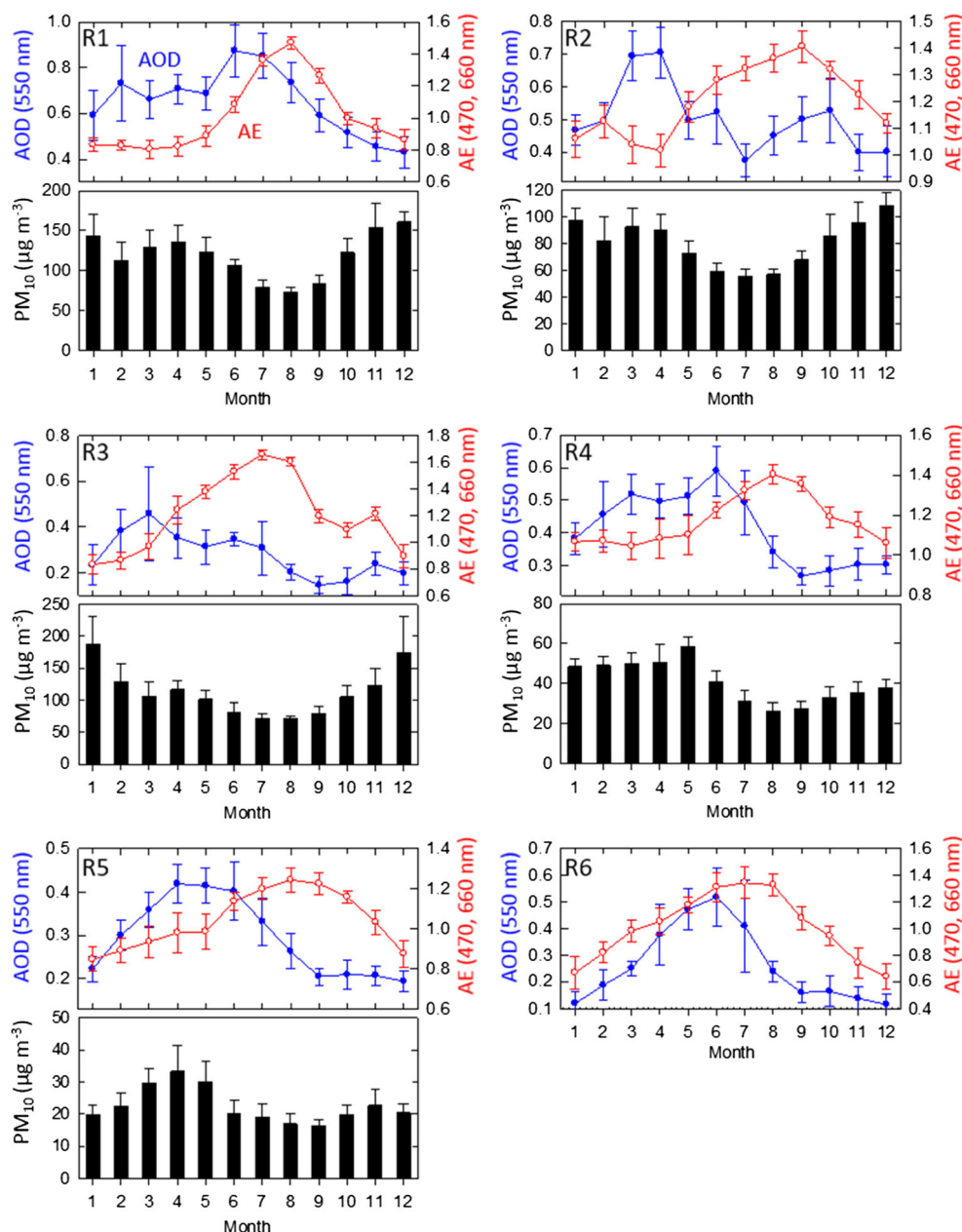
The main features of monthly variations in AOD, ÅE, and PM_{10} concentration for the six regions are as follows (Fig. 2):

1. In North China (R1) and its downwind region (R4), AOD maxima (R1, 0.87 ± 0.11 ; R4, 0.59 ± 0.08) appeared in June due to an accumulation of aerosols under stagnant regional-scale circulation (Figs. 3 and S1). Various processes, such as enhanced secondary aerosol formation, hygroscopic growth of hydrophilic aerosols, and biomass burning aerosols, may also contribute to high AOD during June, as discussed by Kim et al. (2007). ÅE during spring and winter at R1 (0.84 ± 0.07) and R4 (1.07 ± 0.08) were lower than the corresponding values during other seasons in response to the coarse dust particles transported from Inland China and Mongolia (Shao and Dong 2006; Logan et al. 2013). Contrary to AOD, elevated PM_{10} concentrations were apparent from October to June over R1 and

from January to May over R4. This is attributable to the increase of fossil fuel usage for residential heating (Qu et al. 2010), as well as an accumulation of air pollutants under slow-moving, high-pressure systems, and intensive temperature inversion during colder months (Chan and Yao 2008; Xie et al. 2015). The invasion of wind-blown Asian dust is another important factor affecting ground-level PM_{10} concentration.

2. The peak in AOD during March–April (0.70 ± 0.07 ; see also Fig. S1) in South China (R2) appeared 3 months earlier than in R1. This is associated with the accumulated air pollutants under a stagnant, high-pressure system (Fig. S2). The frequent burning of agricultural wastes in R2 is thought to be another possible reason for high AOD during March–April (Fig. 3; van der Werf et al. 2010). From May, however, AOD in R2 decreased to approximately 0.37–0.52 due to frequent precipitation (Fig. S2). Monthly mean ÅE over R2 ranged from 1.0 to 1.4, with a peak on September (1.41 ± 0.06). The overall mean ÅE of 1.20 ± 0.14 at R2 was slightly higher than that of R1 (1.01 ± 0.23) because the influence of Asian dust is slightly less in R2 (Shao and Dong 2006). Meanwhile, an almost identical monthly variation of PM_{10} concentration was observed between R1 and R2, although PM_{10} concentration over R2 ($80 \pm 20 \mu\text{g m}^{-3}$) was lower than that over R1 ($119 \pm 33 \mu\text{g m}^{-3}$).
3. In Northeast China (R3), the maximum AOD of 0.46 ± 0.21 occurred during March with a relatively low

Fig. 2 Monthly variation of MODIS-derived AOD at 550 nm (blue closed circles), ÅE at wavelength 470–660 nm (red open circles), and PM₁₀ (bar) with one standard deviation error bar for six regions



ÅE (0.97 ± 0.10) due to the strong influence of Asian dust transported from inland China and Mongolia (Shao and Dong 2006). A monotonous increase in ÅE from April (1.24 ± 0.11) to July (1.66 ± 0.04) is attributable to the changes of wind direction from northwesterly to southwesterly, leading to significant increase of transported fine particles from R1 (Figs. S1 and S2). Distinct increase of PM₁₀ concentration was found during December–January (mean $181 \pm 49 \mu\text{g m}^{-3}$).

- In the East Sea and Japan (R5), AOD showed consistent increase from January to April, followed by a consistent decrease. The monthly variation in ÅE was quite similar to those at R1 and R4. The overall mean PM₁₀ concentration was estimated as $23 \pm 7 \mu\text{g m}^{-3}$, with a distinct

increase in March–May due to the influence of Asian dust (Shao and Dong 2006).

- Over the Sea of Okhotsk (R6), increased AOD was apparent during April–June, peaking in June (0.52 ± 0.11). This increase in AOD can be explained by Siberian smoke drifts across R3 and Russia to the Sea of Okhotsk (Cottle et al. 2014).

Observed trends in AOD and ÅE

Figure 4 shows time series of monthly mean AOD/ÅE and its trends for the six selected regions. Monthly mean AOD from

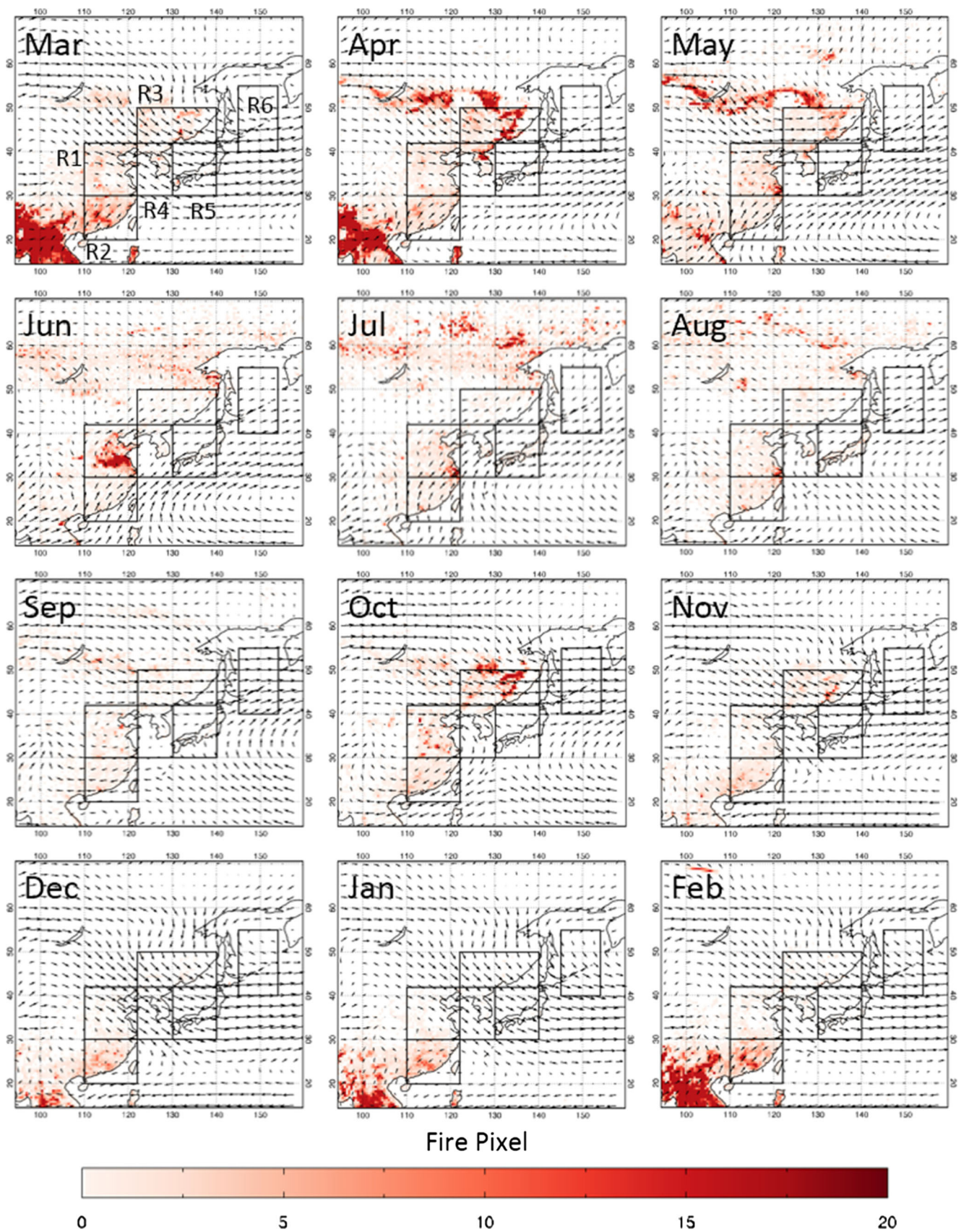
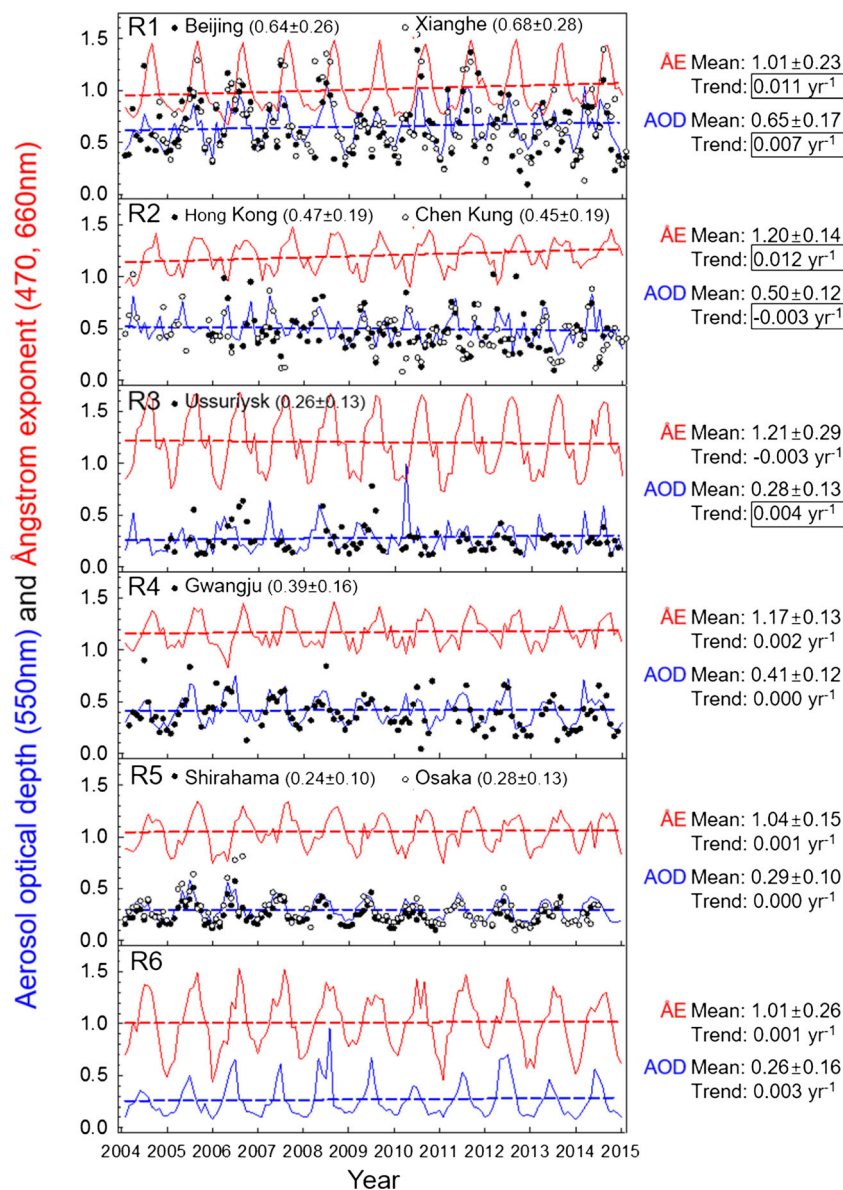


Fig. 3 Spatial distributions of monthly averaged MODIS-derived fire pixel counts, and wind vectors at 850-hPa pressure level over East Asia during 2004–2014. Black boxes indicate the six selected regions given in Fig. 1

Fig. 4 Time series of monthly mean MODIS AOD (blue solid line) and ÅE (red solid line) for six selected regions. The dashed lines are LMS regression fit to the data. The monthly mean values of AOD with one standard deviation from AERONET sun/sky radiometer at Beijing and Xianghe (R1), Hong Kong and Chen Kung (R2), Ussuriysk (R3), Gwangju (R4), and Shirahama and Osaka (R5) are superimposed

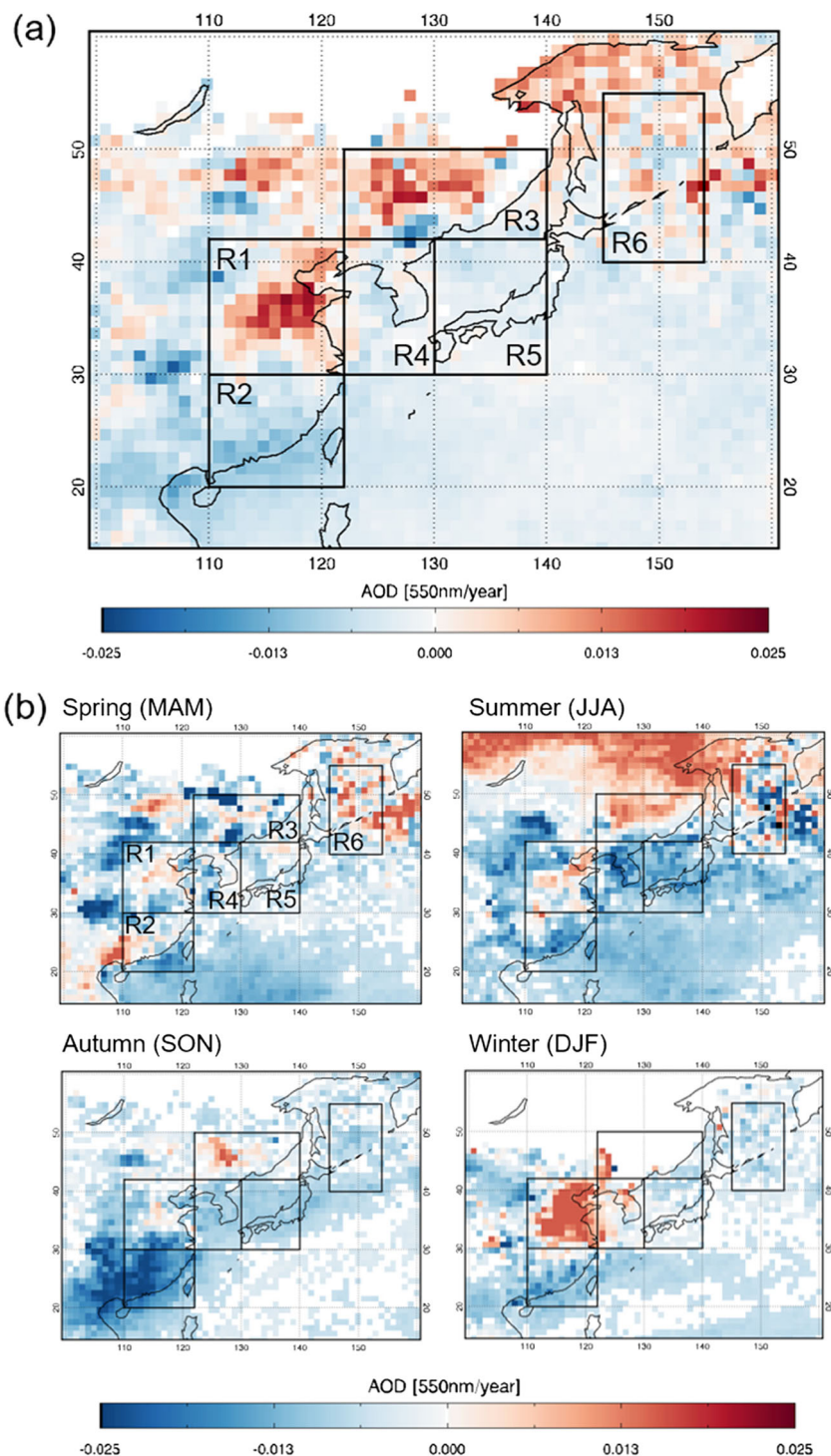


AERONET Cimel sun/sky radiometer measurements in each region is also plotted. The monthly variation in AOD was very similar between MODIS and AERONET for all regions. Spatial distributions of annual and seasonal MODIS AOD trends for the period 2004–2014 are shown in Fig. 5. Note that the trends discussed in Figs. 4 and 5 are statistically significant at the 95% confidence level.

In R1, significantly increasing trends were found for both AOD (+ 1.02% year⁻¹) and ÅE (+ 1.06% year⁻¹). AOD exhibited an especially strong increasing trend (+ 3.96% year⁻¹) in megacities and heavily industrialized areas during winter. This increase is associated with elevated emissions of sulfate as well as other chemical species due to increased coal burning for residential heating during cold months (Chan and Yao 2008; Lalitaporn et al. 2013; Wang et al. 2005). We found a decreasing

AOD trend in R2 (− 0.60% year⁻¹), especially over the coastal regions, in all seasons except spring; in contrast, ÅE in R2 showed an increasing trend (+ 0.96% year⁻¹). AOD trends remain significantly positive in R3, but no clear trends in ÅE are observed in the 11-year dataset. The increasing trend in AOD was observed only during summer, which might be related to transport of pollution particles from R1 by seasonal southeasterly winds, as discussed in the “Spatial and temporal variations in AOD and PM₁₀ concentration” section (Figs. 3 and 5b). Although no significant trends were found for AOD and ÅE in R4, R5, or R6, the pattern of declining AOD over R4 and R5 during summer and autumn generally matched heavy precipitation regions. In the case of R6, AOD showed an increasing trend during spring, which is mainly due to pollution and biomass burning aerosols transported from R3 and Russia.

Fig. 5 Spatial distribution of **a** annual and **b** seasonal MODIS AOD trends for every $1^\circ \times 1^\circ$ during 2004–2014 over East Asia



Changes in column AOD and surface PM_{10} concentration: a comparison

Table 1 summarizes the means and trends for MODIS AOD and PM_{10} concentration at 33 selected stations (R1, 15 urban stations; R2, 10 urban stations; R3, 2 urban stations; R4, 1 urban and 2 background stations; and R5, 3 background stations) over the period 2004–2011.

In R1, AOD showed an increasing trend of $+0.64\% \text{ year}^{-1}$, whereas PM_{10} concentration decreased ($-2.60\% \text{ year}^{-1}$) at five urban sites in the Bohai Sea economic rim (#3 Beijing, #4 Tianjin, #5 Dalian, #6 Yantai, and #7 Qingdao), where mean AOD and PM_{10} concentration were observed to lie within the ranges 0.57–0.83 and 76–185 $\mu\text{g m}^{-3}$, respectively. Five stations (#10 Nanjing, #11 Nantong, #12 Suzhou, #13 Shanghai, and #14 Hangzhou) located in the northern part of the Yangtze River

Table 1 Mean and trend estimates of MODIS-derived AOD and PM₁₀ concentration over the period 2004–2011. For calculating the AOD trend of each station, monthly MODIS AOD was used for each 1° grid scale encompassing each selected station. Italicized numbers indicate trends that are statistically significant at the 95% confidence level

Region	Station	AOD (550 nm)		PM ₁₀ concentration		
		Mean ± SD	Trend [year ⁻¹] (% year ⁻¹)	Mean ± SD	Trend [μg m ⁻³ year ⁻¹] (% year ⁻¹)	
R1N. China	#1	Zhengzhou	0.97 ± 0.33	<i>0.039 (4.39)</i>	119.2 ± 36.0	- 0.73 (- 0.54)
	#2	Shijiazhuang	0.81 ± 0.38	<i>0.015 (1.83)</i>	142.7 ± 59.7	- 8.63 (- 4.47)
	#3	Beijing	0.83 ± 0.33	<i>0.012 (1.43)</i>	185.1 ± 66.8	- 10.42 (- 4.22)
	#4	Tianjin	0.82 ± 0.31	<i>0.020 (2.51)</i>	124.1 ± 44.7	- 3.99 (- 2.60)
	#5	Dalian	0.59 ± 0.21	0.000 (0.03)	85.9 ± 25.2	- 4.29 (- 3.83)
	#6	Yantai	0.57 ± 0.20	0.006 (0.93)	76.1 ± 22.0	<i>2.13 (2.92)</i>
	#7	Qingdao	0.69 ± 0.21	0.006 (0.79)	106.3 ± 35.5	- 0.44 (- 0.37)
	#8	Lianyungang	0.80 ± 0.24	<i>0.015 (1.89)</i>	103.8 ± 37.5	- 1.02 (- 0.86)
	#9	Hefei	0.81 ± 0.24	<i>0.007 (0.76)</i>	131.5 ± 51.5	<i>4.59 (3.70)</i>
	#10	Nanjing	0.80 ± 0.26	<i>0.023 (2.96)</i>	127.8 ± 44.8	- 3.47 (- 2.25)
	#11	Nantong	0.90 ± 0.25	<i>0.022 (2.46)</i>	100.5 ± 38.8	- 2.66 (- 2.21)
	#12	Suzhou	0.95 ± 0.23	<i>0.018 (1.84)</i>	111.1 ± 40.9	- 4.73 (- 3.33)
	#13	Shanghai	0.88 ± 0.23	<i>0.022 (2.47)</i>	97.9 ± 38.6	- 3.67 (- 3.00)
	#14	Hangzhou	0.85 ± 0.21	<i>0.015 (1.76)</i>	124.1 ± 47.8	- 6.48 (- 3.95)
	R2 S. China	#15	Wuhan	0.89 ± 0.22	<i>0.010 (1.03)</i>	140.4 ± 59.8
#16		Changsha	0.72 ± 0.19	0.000 (0.04)	125.3 ± 56.3	- 14.64 (- 7.31)
#17		Nanchang	0.79 ± 0.19	0.003 (0.29)	93.4 ± 24.8	- 0.93 (- 0.87)
#18		Guilin	0.64 ± 0.20	- 0.008 (- 1.02)	52.4 ± 18.6	<i>4.58 (12.14)</i>
#19		Ningbo	0.54 ± 0.18	0.002 (0.27)	100.6 ± 44.9	<i>2.43 (2.42)</i>
#20		Wenzhou	0.46 ± 0.13	0.001 (0.19)	81.6 ± 22.4	<i>3.18 (4.23)</i>
#21		Fuzhou	0.41 ± 0.13	- 0.002 (- 0.36)	71.4 ± 17.5	- 0.75 (- 0.92)
#22		Xiamen	0.49 ± 0.19	- 0.005 (- 0.81)	67.5 ± 19.4	- 0.33 (- 0.45)
#23		Shantou	0.51 ± 0.19	- 0.007 (- 1.16)	61.4 ± 18.5	- 0.22 (- 0.32)
#24		Shenzhen	0.47 ± 0.17	- 0.008 (- 1.40)	64.6 ± 23.0	- 2.49 (- 3.06)
#25		Guangzhou	0.70 ± 0.21	- 0.010 (- 1.22)	85.1 ± 28.7	- 6.15 (- 5.15)
R3NE. China	#26	Changchun	0.40 ± 0.17	<i>0.029 (9.34)</i>	104.9 ± 38.4	- 2.38 (- 1.91)
	#27	Harbin	0.40 ± 0.38	<i>0.040 (15.11)</i>	119.7 ± 54.3	- 2.71 (- 1.91)
R4Korea	#28	Seoul	0.53 ± 0.20	0.001 (0.10)	59.1 ± 20.2	- 4.27 (- 5.15)
	#29	Anmyon	0.48 ± 0.19	0.000 (0.07)	38.0 ± 10.5	- 0.02 (- 0.04)
	#30	Gosan	0.38 ± 0.12	<i>0.008 (1.98)</i>	29.8 ± 9.0	- 0.01 (- 0.04)
R5Japan	#31	Yusuhara	0.30 ± 0.10	0.003 (0.88)	18.7 ± 6.8	- 0.64 (- 2.77)
	#32	Oki	0.33 ± 0.14	0.000 (0.11)	27.5 ± 9.3	- 0.38 (- 1.20)
	#33	Sado-seki	0.29 ± 0.11	0.001 (0.24)	23.2 ± 7.1	- 0.78 (- 2.74)

Delta economic rim showed increasing AOD trend (+ 1.32% year⁻¹), but decreasing PM₁₀ concentration trend (- 2.83% year⁻¹), which were about two times greater than those of five sites in the Bohai Sea economic rim. PM₁₀ concentration showed positive trend (+ 3.51% year⁻¹) at two urban stations (#19 Ningbo and #20 Wenzhou) in the southern part of the Yangtze River Delta economic rim, although no trend was observed in AOD for either site. The AOD trend in the mid-Yangtze River region was estimated as + 0.76% year⁻¹ at #9 Hefei and + 1.03% year⁻¹ at #15 Wuhan. The PM₁₀ concentration trends

were negative at Wuhan (- 4.05% year⁻¹), #16 Changsha (- 7.31% year⁻¹), and #17 Nanchang (- 0.87% year⁻¹). However, we cannot explain the positive trend in PM₁₀ concentration observed at Hefei (+ 3.70% year⁻¹).

We found decreasing trends in both AOD (- 1.32% year⁻¹) and PM₁₀ concentration (- 0.77% year⁻¹) for three stations (#21 Fuzhou, #22 Xiamen, and #23 Shantou) along the south-east coast of R2. Two stations located near the Pearl River Delta economic rim in R2 (#24 Shenzhen and #25 Guangzhou) have much larger declining trends in AOD

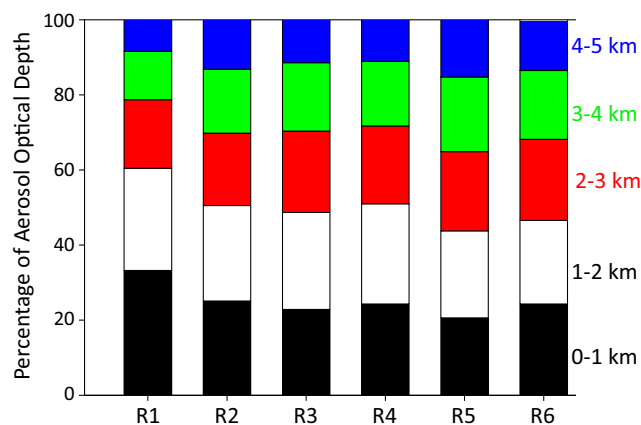


Fig. 6 AOD percentage per kilometer altitude for each region, estimated from space-borne lidar CALIOP measurements from 2007 to 2014

(-2.21% year $^{-1}$) and PM_{10} concentration (-4.23% year $^{-1}$) than the other sites in R2.

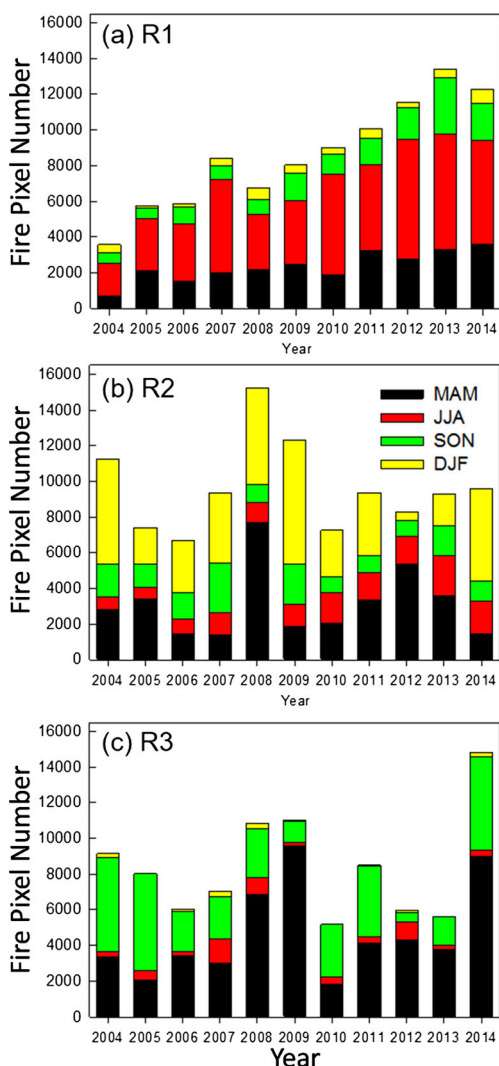


Fig. 7 Annual variation in fire pixel number from 2004 to 2014 for three regions: **a** R1 (North China), **b** R2 (South China), and **c** R3 (Northeast China)

In R3, positive AOD ($+8.10\%$ year $^{-1}$) and negative PM_{10} concentration (-2.28% year $^{-1}$) trends were found at two stations (#26 Changchun and #27 Harbin). In R4, only background site (#30 Gosan) showed significant increasing trend in AOD ($+1.98\%$ year $^{-1}$); however, considerable changes in PM_{10} concentration (-5.15% year $^{-1}$) were observed at urban site (#28 Seoul). No significant trends were found for background stations (#31 Yusu-hara, #32 Oki, and #33 Sado-seki) in Japan (R5), with the exception of the PM_{10} concentration trend (-2.74% year $^{-1}$) at Sado-seki station.

Overall, 18 of the 20 stations in R1, R3, and R4 showed positive AOD trends, but significantly declining PM_{10} concentrations were still observed during 2004–2011. Here, we should note that observed trends in both AOD and PM_{10} concentrations at 12 out of 18 stations were statistically significant at the 95% confidence level. The possible reasons for this contradictory trend between AOD and PM_{10} concentration at 18 out of 20 stations are described as follows:

1. The reductions of coarse particle emissions (e.g., suspended fugitive dust) in megacities, enforced by strict policies on reducing air pollution (e.g., Action Plan for Air Pollution Prevention and Control), can directly reduce ground-level PM_{10} concentrations. However, several studies has reported no significant changes in $\text{PM}_{2.5}$ concentrations in megacities in China due to continuous primary fine particle emissions and secondary particle formation (Lang et al. 2017; Lv et al. 2016; Xie et al. 2015; Zheng et al. 2015). This implies that AOD, which is defined as an integral of aerosol extinction coefficient with altitude, has also remained stable or has increased slightly in response to the amount of submicron particles, which have high light-extinction efficiency (Seinfeld et al. 1998).
2. AOD is determined by the aerosols distributed within a column of air, that is, in and above the atmospheric boundary layer. Figure 6 shows the percentage of AOD for every kilometer from the surface to 5 km altitude for the six selected regions, which derived from space-borne lidar Cloud-Aerosol Lidar with Orthogonal Polarization (CALIOP) measurements onboard Cloud-Aerosol Lidar and Infrared Pathfinder Satellite Observations (CALIPSO). The percentage of AOD from the surface to 1 km was approximately 33% (60% at 2 km) in R1. Similar ratios were also observed in other regions. As indicated in Fig. 6, large amounts of aerosols remain in the free troposphere, which does seem to affect AOD measurements.
3. Increased fine particle emissions from biomass burning activities in R1 may contribute to AOD more than to surface PM_{10} concentration, due to its favorable size for scattering light. Figure 7 shows annual mean MODIS-derived fire counts over three regions. Although

accumulated fire counts in R2 and R3 showed large annual and inter-annual variations, no statistically significant trend in fire counts was found. However, R1 showed distinct increasing trend, especially during summer. Thus, increased emission of aerosols from biomass burning can be attributed to the positive AOD trend shown in R1 (Fig. 5).

Meanwhile, as mentioned in the “Observed trends in AOD and AE ” section, no coherent trends for PM_{10} concentration were found among stations in R2 although trends for AOD were declining (Fig. 5 and Table 1). Some possible explanations for these contradictory observations include a trend toward increasing precipitation over R2, which is also accompanied by increases in heavy rainfall, precipitation intensity, and frequency of precipitation events (Awan et al. 2015; Duan et al. 2013).

Summary and conclusion

Multi-year records of AOD and PM_{10} concentration for six selected regions of interest in East Asia were analyzed for spatio-temporal variations and trends.

Different features of monthly/seasonal variations in both AOD and PM concentration were observed among the selected regions, which were associated with distinct changes in regional-scale seasonal circulations. Enhanced AOD over North China and its downwind regions (Yellow Sea and Korea) appeared in June, compared with March–April over South China. Increased PM_{10} concentrations in both North and South China were observed from late fall to spring. In Northeast China, AOD peaked during March, whereas high PM_{10} concentrations occurred during December–January.

A considerable decreasing trend in both AOD and PM_{10} concentration was observed in South China, which is potentially related to increased precipitation. However, a significant increasing trend in AOD was found in North China and Northeast China (particularly in 18 out of 20 megacities), whereas surface PM_{10} concentrations over most megacities in these two regions declined almost linearly. The reductions in PM_{10} concentrations can be attributed to large reductions in the emission of near-surface coarse particles due to a series of strict control measures. However, an increase in AOD indicates that highly scattering submicron secondary particles have not been meaningfully reduced. Space-borne lidar CALIOP measurements revealed that approximately 60–70% of AOD was contributed by the aerosols present above the atmospheric boundary layer (> 1 km altitude).

Our findings suggest that strict restrictions on the emission of $\text{PM}_{2.5}$ and its precursor gaseous are required in order to improve particulate air quality and to reduce

adverse human health effect, so as to further reduce their radiative effects. Especially, further studies on the physicochemical and optical characteristics of fine particles (i.e., $\text{PM}_{2.5}$) are needed to develop effective strategies and actions for reducing these effects, although we have not addressed recent changes in $\text{PM}_{2.5}$ concentrations over East Asia due to the lack of continuous observations at multiple locations.

Acknowledgements We thank the principle investigators at Aerosol Robotic Network (AERONET) and the Moderate Resolution Imaging Spectroradiometer (MODIS) and Cloud-Aerosol Lidar and Infrared Pathfinder Satellite Observations (CALIPSO) project offices for enabling easy access to the data.

Funding information This study was supported by the Korean Meteorological Administration (KMA) Research and Development Program under Grant KMIPA 2015–2011 and the Korean Ministry of Environment as “Climate Change Correspondence”.

References

- Awan JA, Bae DH, Kim KJ (2015) Identification and trend analysis of homogeneous rainfall zones over the East Asia monsoon region. *Int J Climatol* 35:1422–1433
- Cai W, Li K, Liao H, Wang H, Wu L (2017) Weather conditions conducive to Beijing severe haze more frequent under climate change. *Nat Clim Chang* 7:257–262
- Chan CK, Yao XH (2008) Air pollution in mega cities in China. *Atmos Environ* 42:1–42
- Cheng Z, Jiang JK, Fajardo O, Wang SX, Hao JM (2013) Characteristics and health impacts of particulate matter pollution in China (2001–2011). *Atmos Environ* 65:186–194. <https://doi.org/10.1016/j.atmosenv.2012.10.022>
- Chew BN, Campbell JR, Hyer EJ, Salinas SV, Reid JS, Welton EJ, Holben BN, Liew SC (2016) Relationship between aerosol optical depth and particulate matter over Singapore: effects of aerosol vertical distributions. *Aerosol Air Qual Res* 16:2818–2830
- Collaud Coen M, Andrews E, Asmi A, Baltensperger U, Bukowiecki N, Day D, Fiebig M, Fjaeraa AM, Flentje H, Hyvärinen A, Jefferso A, Jennings SG, Kouvarakis G, Lihavainen H, Lung Myhre C, Malm WC, Mihapopoulous N, Molenaar JV, O’Dowd C, Ogren JA, Schichtel BA, Sheridan P, Virkkula A, Weingartner E, Weller R, Laj P (2013) Aerosol decadal trends—part 1: in-situ optical measurements at GAW and IMPROVE stations. *Atmos Chem Phys* 13:869–894
- Cottle P, Strawbridge K, McKendry I (2014) Long-range transport of Siberian wildfire smoke to British Columbia: Lidar observations and air quality impacts. *Atmos Environ* 90:71–77
- Duan A, Wang M, Lei Y, Cui Y (2013) Trends in summer rainfall over China associated with the Tibetan Plateau sensible heat source during 1980–2008. *J Clim* 26:261–275. <https://doi.org/10.1175/jcli-d-11-00669.1>
- Engel-Cox JA, Hoff RM, Rogers R, Dimmick F, Rush AC, Szykman JJ, Al-Saadi J, Chu DA, Zell ER (2006) Integrating lidar and satellite optical depth with ambient monitoring for 3-dimensional particulate characterization. *Atmos Environ* 40:8056–8067
- Kim S-W, Yoon SC, Kim J, Kim S-Y (2007) Seasonal and monthly variations of columnar aerosol optical properties over east Asia

- determined from multi-year MODIS, LIDAR, and AERONET sun/sky radiometer measurements. *Atmos Environ* 41:1634–1651
- Kim S-W, Yoon SC, Kim J (2008) Columnar Asian dust particle properties observed by sun/sky radiometers from 2000 to 2006 in Korea. *Atmos Environ* 42:492–504
- Kim HS, Chung YS, Yoon MB (2016) An analysis on the impact of large-scale transports of dust pollution on air quality in East Asia as observed in central Korea in 2014. *Air Qual Atmos Health* 9:83–93
- Lalitaporn P, Kurata G, Matsuoka Y, Thongboonchoo N, Surapipith V (2013) Long-term analysis of NO₂, CO, and AOD seasonal variability using satellite observations over Asia and intercomparison with emission inventories and model. *Air Qual Atmos Health* 6(4): 655–672
- Lang J, Zhang Y, Zhou Y, Cheng S, Chen D, Guo X, Chen S, Li X, Xing X, Wang H (2017) Trends of PM_{2.5} and chemical composition in Beijing, 2000–2015. *Aerosol Air Qual Res* 17:412–425
- Levy RC, Mattoo S, Munchak LA, Remer LA, Sayer AM, Patadia F, Hsu NC (2013) The collection 6 MODIS aerosol products over land and ocean. *Atmos Meas Technol* 6:2989–3034
- Liu Q, Baumgartner J, Zhang Y, Schauer JJ (2016) Source apportionment of Beijing air pollution during a severe winter haze event and associated pro-inflammatory responses in lung epithelial cells. *Atmos Environ* 126:28–35
- Logan T, Xi B, Dong X, Li Z, Cribb M (2013) Classification and investigation of Asian aerosol absorptive properties. *Atmos Chem Phys* 13:2253–2265
- Lu W, Yang L, Chen J, Wang X, Li H, Zhu Y, Wen L, Xu C, Zhang J, Zhu T, Wang W (2016) Identification of concentrations and sources of PM_{2.5} 5-bound PAHs in North China during haze episodes in 2013. *Air Qual Atmos Health* 9:823–833
- Lv B, Hu Y, Chang HH, Russell AG, Bai Y (2016) Improving the accuracy of daily PM_{2.5} distributions derived from the fusion of ground-level measurements with aerosol optical depth observations, a case study in North China. *Environ Sci Technol* 50:4752–4759
- Ma Z, Hu X, Huang L, Bi J, Liu Y (2014) Estimating ground-level PM_{2.5} in China using satellite remote sensing. *Environ Sci Technol* 48: 7436–7444
- Mehta S, Shin H, Burnett R, North T, Cohen AJ (2013) Ambient particulate air pollution and acute lower respiratory infections: a systematic review and implications for estimating the global burden of disease. *Air Qual Atmos Health* 6:69–83
- Nguyen DL, Kim JY, Ghim YS, Shim SG (2015) Influence of regional biomass burning on the highly elevated organic carbon concentrations observed at Gosan, South Korea during a strong Asian dust period. *Environ Sci Pollut Res* 22:3594–3605
- O'Neill MS, Breton CV, Devlin RB, Utell MJ (2012) Air pollution and health: emerging information on susceptible populations. *Air Qual Atmos Health* 5:189–201
- Oberdörster G, Oberdörster E, Oberdörster J (2005) Nanotoxicology: an emerging discipline evolving from studies of ultrafine particles. *Environ Health Perspect* 113:823–839
- Peel JL, Haeuber R, Garcia V, Russell AG, Neas L (2013) Impact of nitrogen and climate change interactions on ambient air pollution and human health. *Biogeochemistry* 114:121–134
- Pozzer A, de Meij A, Yoon J, Tost H, Georgoulias AK, Astitha M (2015) AOD trends during 2001–2010 from observations and model simulations. *Atmos Chem Phys* 15:5521–5535
- Qu WJ, Arimoto R, Zhang XY, Zhao CH, Wang YQ, Sheng LF, Fu G (2010) Spatial distribution and interannual variation of surface PM₁₀ concentrations over eighty-six Chinese cities. *Atmos Chem Phys* 10:5641–5662. <https://doi.org/10.5194/acp-10-5641-2010>
- Remer LA, Kaufman YJ, Tanre D, Mattoo S, Chu DA, Martins JV, Li RR, Ichoku C, Levy RC, Kleidman RG, Eck TF, Vermote E, Holben BN (2005) The MODIS aerosol algorithm, products, and validation. *J Atmos Sci* 62:947–973. <https://doi.org/10.1175/JAS3385.1>
- Schulz M, Textor C, Kinne S, Balkanski Y, Bauer S, Bernsten T, Berglen T, Boucher O, Dentener F, Guibert S, Isaksen ISA, Iversen T, Koch D, Kirkevåg A, Liu X, Montanaro V, Myhre G, Penner JE, Pitari G, Reddy S, Seland Ø, Stier P, Takemura T (2006) Radiative forcing by aerosols as derived from the AeroCom present-day and pre-industrial simulations. *Atmos Chem Phys* 6:5225–5246
- Seinfeld JH, Pandis SN, Noone K (1998) Atmospheric chemistry and physics: from air pollution to climate change. Wiley-Interscience Publication, Hoboken
- Seo S, Kim J, Lee H, Jeong U, Kim W, Holben BN, Kim S-W, Song CH, Lim JH (2015) Estimation of PM₁₀ concentrations over Seoul using multiple empirical models with AERONET and MODIS data collected during the DRAGON-Asia campaign. *Atmos Chem Phys* 15: 319–334
- Shao Y, Dong CH (2006) A review of East Asian dust storm climate, modelling and monitoring. *Glob Planet Chang* 52:1–22
- Shindell DT, Lamarque J-F, Schulz M, Flanner M, Jiao C, Chin M, Young PJ, Lee YH, Rotstayn L, Mahowald N, Milly G, Faluvegi G, Balkanski Y, Collins WJ, Conley AJ, Dalsoren S, Easter R, Ghan S, Horowitz L, Liu X, Myhre G, Nagashima T, Naik V, Rumbold ST, Skeie R, Sudo K, Szopa S, Takemura T, Voulgarakis A, Yoon J-H, Lo F (2013) Radiative forcing in the ACCMIP historical and future climate simulations. *Atmos Chem Phys* 13:2939–2974
- Streets DG, Yan R, Chin M, Diehl T, Mahowald N, Schultz M, Wild M, Wu Y, Yu C (2009) Anthropogenic and natural contributions to regional trends in aerosol optical depth, 1980–2006. *J Geophys Res* 114(D10).doi:<https://doi.org/10.1029/2008JD011624>
- Tiao GC, Reinsel GC, Xu D, Pedrick JH, Zhu X, Mler AJ, DeLuisi JJ, Mateer CL, Wuebbles DJ (1990) Effects of autocorrelation and temporal sampling schemes on estimates of trend and spatial correlation. *J Geophys Res* 95(D12)
- van der Werf GR, Randerson JT, Giglio L, Collatz GJ, Mu M, Kasibhatla PS, Morton DC, DeFries RS, Jin Y, van Leeuwen TT (2010) Global fire emissions and the contribution of deforestation, savanna, forest, agricultural, and peat fires (1997–2009). *Atmos Chem Phys* 10: 11707–11735. <https://doi.org/10.5194/acp-10-11707-2010>
- Wang H-J, Chen H-P (2016) Understanding the recent trend of haze pollution in eastern China: roles of climate change. *Atmos Chem Phys* 16:4205–4211. <https://doi.org/10.5194/acp-16-4205-2016>
- Wang Y, Zhuang G, Tang A, Yuan H, Sun Y, Chen S, Zheng A (2005) The ion chemistry and the source of PM_{2.5} aerosol in Beijing. *Atmos Environ* 39:3771–3784
- Wang SX, Zhao B, Cai SY, Klimont Z, Nielsen CP, Morikawa T, Woo JH, Kim Y, Fu X, Xu JY, Hao JM, He KB (2014) Emission trends and mitigation options for air pollutants in East Asia. *Atmos Chem Phys* 14:6571–6603
- Weatherhead EC, Reinsel GC, Tiao GC, Meng X-L, Choi D, Cheang W-K, Keller T, DeLuisi J, Wuebbles DJ, Kerr JB, Miller AJ, Oltmans SJ, Frederick JE (1998) Factors affecting the detection of trends: statistical considerations and applications to environmental data. *J Geophys Res* 103:17149–17161. <https://doi.org/10.1029/98JD00995>
- Xie Y, Bin Z, Lin Z, Rong L (2015) Spatiotemporal variations of PM_{2.5} and PM₁₀ concentrations between 31 Chinese cities and their relationships with SO₂, NO₂, CO and O₃. *Particuology* 20:141–149
- Yin D, Zhao S, Qu J (2017) Spatial and seasonal variations of gaseous and particulate matter pollutants in 31 provincial capital cities, China. *Air Qual Atmos Health* 10:359–370
- You W, Zang Z, Zhang L, Li Z, Chen D, Zhang G (2015) Estimating ground-level PM₁₀ concentration in northwestern China using geographically weighted regression based on satellite AOD combined with CALIPSO and MODIS fire count. *Remote Sens Environ* 168: 276–285
- Yu X, Zhu B, Yin Y, Yang J, Li Y, Bu X (2011) A comparative analysis of aerosol properties in dust and haze-fog days in a Chinese urban region. *Atmos Res* 99:241–247

- Zhang J, Reid JS (2010) A decadal regional and global trend analysis of the aerosol optical depth using a data-assimilation grade over-water MODIS and level 2 MISR aerosol products. *Atmos Chem Phys* 10: 10949–10963
- Zhang XY, Gong SL, Shen ZX, Mei FM, Xi XX, Liu LC, Zhou ZJ, Wang D, Wang YQ, Cheng Y (2003) Characterization of soil dust aerosol in China and its transport/distribution during 2001 ACE-Asia:1. Network observations. *J Geophys Res* 108(D9):4261
- Zhang X, Wang L, Wang W, Cao D, Wang X, Ye D (2015) Long-term trend and spatiotemporal variations of haze over China by satellite observations from 1979 to 2013. *Atmos Environ* 119:362–373
- Zheng S, Pozzer A, Cao CX, Lelieveld J (2015) Long-term (2001–2012) concentrations of fine particulate matter (PM_{2.5}) and the impact on human health in Beijing, China. *Atmos Chem Phys* 15:5715–5725